Retuning of hippocampal representations during sleep

Kamran Diba (kdiba@umich.edu)
University of Michigan https://orcid.org/0000-0001-5128-4478
Kourosh Maboudi
University of Michigan
Bapun Giri
University of Michigan
Hiroyuki Miyawaki
Osaka City University Graduate School of Medicine https://orcid.org/0000-0003-1556-1348
Caleb Kemere
Rice University https://orcid.org/0000-0003-2054-0234

Biological Sciences - Article

Keywords:

Posted Date: November 7th, 2022

DOI: https://doi.org/10.21203/rs.3.rs-2191626/v1

Additional Declarations: There is **NO** Competing Interest.

Retuning of hippocampal representations during sleep

Kourosh Maboudi (1,2), Bapun Giri (1,2), Hiroyuki Miyawaki (2,3), Caleb Kemere (4), Kamran Diba (1)

Affiliations

(1) Dept of Anesthesiology and Neuroscience Graduate Program, University of Michigan, Ann Arbor, MI 48103
(2) Dept of Psychology, University of Wisconsin-Milwaukee, Milwaukee, WI 53211
(3) Present address: Osaka Metropolitan University, Osaka, Japan.
(4) Dept of Biomedical Engineering, Rice University, Houston, TX

Abstract

Hippocampal representations that underlie spatial memory undergo continuous refinement following formation during exploration. Understanding the role of sleep in this process has been challenging because of the inaccessibility of place fields when animals are not actively exploring a maze. Here, we used a novel Bayesian learning approach based on the spike-triggered average decoded position in ensemble recordings to track dynamically the spatial tuning of individual neurons during offline states in freely moving rats. Measuring these dynamic tunings, we found spatial representations within hippocampal sharp-wave ripples that were stable for hours during sleep and were strongly aligned with place fields initially observed during maze exploration. These representations were explained by a combination of factors that included the pre-configured structure of firing rates in sleep before exposure to the environment, and representations that emerged during theta oscillations and awake sharp-wave ripples on the maze, revealing the contribution of these events in forming ensembles during sleep. Strikingly, the ripple representations during sleep predicted the future place fields of neurons during re-exposure to the maze, even when those fields deviated from previous place preferences. These observations demonstrate that ripples during sleep drives representational drift observed across maze exposures. In contrast, we observed tunings with poor alignment to maze place fields during other time periods, including in sleep and rest before maze exposure, during rapid eye movement sleep, and following the initial several hours in slow-wave sleep. In sum, the novel decoding approach described here allowed us to infer and characterize the retuning of place fields during offline periods, revealing the rapid emergence of representations following novel exploration and the active role of sleep in the representational dynamics of the hippocampus.

Introduction

Memories are continuously refined after they form. Different stages of sleep play important roles in the transformations that memories undergo, but many aspects of these offline processes remain unknown. Memories that involve the hippocampus are particularly affected by sleep, which alters molecular signaling, excitability and synaptic connectivity of hippocampal neurons [1,2]. Memories are considered to be represented by the activity of ensembles of neurons that form with experience [3]. In the rat hippocampus, these ensembles are tuned to locations within a maze environment [4]. Indeed, an animal's position can be decoded from the spike trains recorded from a population of neurons (**Fig. 1a**)[5]. Spatial representations, however, do not remain stationary following initial formation. In many cases the place fields (PFs) of hippocampal neurons develop and shift during traversals of an environment [6,7], remap upon exposure to different arenas [8], and reset or remap even with repeated exposure to the same place [9,10].

We conjectured that modifications of spatial representations would take place during sleep when connections between some neurons are strengthened while those between other neurons are weakened [1,11]. Consistent with this conjecture, cells that become active in a new environment continue to reactivate for hours during sharp-wave ripples in sleep [12], suggesting that offline processes during sleep involve the spatial representations of hippocampal neurons. Moreover, the collective hippocampal map of space shows changes following sleep [13] and some cells express immediate early genes during this period which can mark them for sleep-dependent processing [14]. However, while spatial representations are readily measured from the spiking activities of neurons when animals explore a maze environment, access to these non-stationary representations is lost when animals cease exploring, making it challenging to evaluate how spatial representations are shaped over time.

To evaluate and track the spatial preferences of a neuron across online and offline periods, we developed a novel method based on the principle of Bayesian learning [15] (**Fig. 1b**). Under the assumption of conditional independence of Poisson spike counts from hippocampal neurons conditioned on location, we derived the Bayesian learned tuning (LT) of a neuron from the spike-triggered average of the posterior probability distribution of position determined from the simultaneous spiking patterns of all other neurons in the recorded ensemble, including for time periods when animals are remote from the maze locations for which position was specified. In this formalism, the internally generated preference of a neuron for a location is revealed through its consistent coactivity with other neurons in the ensemble associated with that position.

These Bayesian learned tunings allowed us to track, for the first time, the place-preferences of neurons as they evolved in exceptionally long-duration (up to 14 h) hippocampal unit recordings, enabling us to identify those periods and events in which the firing activities of neurons were consistent or inconsistent with place fields on the maze and to characterize the plastic offline changes in tuning relative to the broader ensemble. This analysis led to multiple novel insights. We found that in sleep following exposure to a maze, hippocampal neurons rapidly reconfigured to provide spatial representations that aligned with the place fields on the maze. Regression analysis revealed that these representations were explained by a combination of factors that included firing patterns pre-configured in pre-exposure sleep, and ensembles that emerged during theta oscillations and awake sharp-wave ripples on the maze, demonstrating the importance of these events in the formation of ensemble patterns in post-maze

sleep. For hours of sleep following the maze, these ripple representations remained stable despite the scarcity of sequential replay trajectories through the maze environment. Remarkably, the representations in sleep predicted the place fields of neurons manifested on repeat exposure to the same maze, including for neurons whose fields deviated from their previous place preferences. Thus, we find that the ensemble firing patterns during ripples account for the representational drift observed across maze exposures [16], demonstrating that drift is not a passive process but instead involves an active processes during sleep. During other time periods, however, such as in sleep and rest before maze exposure, during rapid eye movement sleep, and following the initial several hours of slow-wave sleep, the observed spatial tunings were poorly aligned to the place fields on the maze, highlighting the unique role of sharp-wave ripples in the representational dynamics of hippocampal place fields.

Results

Spatial tunings during ripples in post sleep align with place fields on the maze.

We first examined how tuning curves are impacted by an animal's experience on a maze by characterizing the representations of neurons from spike trains recorded from the rat hippocampus in experiments where rest and sleep in a home cage both preceded (PRE) and followed (POST) exposure to a novel track (MAZE), where rats ran for water reward. To examine spatial tunings in each brain state separately, we first separated unit and local field potential data recorded from hippocampal region CA1 into different states using general criterion (see **Methods**) for rapid eye movement sleep (REM, sleep featuring prominent theta), ripple periods during rest and sleep (150-250 Hz band power accompanied by high multi-unit firing rates), slow-wave sleep (SWS) periods exclusive of ripples, and active wake (with prominent theta). We calculated place fields and the learned tunings for each epoch for all units with peak spatial firing rates > 1 Hz on the maze (**Fig. 2a-c**). We limited the initial analysis to the first 4h of POST, during which we expect greater similarity with maze firing patterns [12]. Learned tunings showed a wide distribution of fidelity to place fields from PRE to POST depending on brain state. Population vector (PV) correlations between spatial bins in place fields and learned tunings (**Fig. 2b**) and LT-PF Pearson correlation coefficients (**Fig. 2c**) demonstrated that the highest fidelities to place fields were observed in spatial representations during theta and ripples on the maze, as expected [17,18]. However, among offline periods only spatial tunings evidenced during POST ripples and non-ripple slow-wave sleep showed significant correlations with unit place fields in MAZE, and notably not those during PRE ripples. Surprisingly, we also failed to find representations consistent with the maze during REM sleep, when vivid dream episodes are frequently experienced [19]. This may reflect that the bulk of REM sleep corresponds only weakly to previous experience [20]. Thus, we find that only during POST slow-wave sleep do place fields maintain internal tunings consistent with their place fields on the maze.

Spatial representations are more stable in post-maze sleep.

We next tracked the learned tunings of neurons over time and examined the consistency of their place preferences within different epochs. We calculated LTs in 15 min windows sliding in 5 min steps during each session, from PRE through MAZE and the first 4 h of POST. Sample unit tunings from a recording session are shown in **Fig. 3a** (additional examples provided in **Extended Data Fig. 1**). These examples show stable LTs for multiple successive time windows during POST, and in some instances, also during PRE. To quantify the LT stability for each unit, we used Pearson correlation coefficients to assess the

consistency of the learned tunings across time windows within and between behavioral epochs (**Fig. 3b**). High off-diagonal values in the correlation matrices within an epoch indicated that the LT remained stable during that epoch. For the example units in **Fig. 3c** we compared the median LT stability values from each epoch against shuffle distributions generated by randomizing the unit identities of the LTs at each time window. This z-scored LT stability was > 0 in both PRE and POST in this session (**Fig. 3d**) and for data pooled across all sessions (**Fig. 3e**), but it was significantly higher in POST compared to PRE, revealing that POST sleep representations were more stable than those in PRE. When we measured the LT stability across time windows from PRE to POST epochs, to examine their consistency from before and after the novel maze exposure when place fields first form, the PRE w/ POST LT stability was significantly > 0 in the example session (median = 0.58, $p = 0.02$) as well as in the pooled data (median = 0.66 , $p < 10^{-11}$, Wilcoxon signed rank test (WSRT, n = 682)) but this was significantly lower than the stabilities observed within PRE and POST (PRE vs PRE w/ POST: $z = 13.2$, $p < 10^{-39}$; POST vs PRE w/ POST: $z = 18.4$, $p < 10^{-75}$, WSRT (n = 682)), signaling that only a small minority of units maintained the same consistent spatial tuning from before to after maze exposure.

A subset of units showed remarkably stable learned tunings during PRE which compelled us to consider whether the LTs of those units might show higher fidelity with maze PFs. To test this conjecture, we divided units into "stable" and "unstable" by whether their z-scored LT stability was > or < 2 (PRE: 379 stable vs 304 unstable; POST:491 stable vs 192 unstable), respectively, in both PRE and POST. In POST, units with both stable and unstable LTs showed significant PF fidelity ($p < 10^{-4}$, comparison against 10000 unit identity shuffles). However, the PF fidelity of units with stable LTs was significantly higher compared to units with unstable LTs in POST. Importantly, in PRE there was no significant difference between PF fidelities of stable and unstable units, and neither of these subsets showed significantly greater PF fidelity compared to a surrogate distribution obtained by shuffling unit identities (stable LTs: $p = 0.58$; unstable LTs: $p = 0.54$). Furthermore, we found little alignment with maze place fields even during ripple events in PRE that featured high replay scores (**Extended Data Fig. 2**). These findings demonstrate that although some units in PRE display stable learned spatial tunings, these tunings do not typically anticipate the future place fields of these neurons but rather show a broad distribution of alignments with the maze place preferences. In contrast, both the low score and high score LTs from MAZE and POST showed strong fidelity to maze PFs, despite the absence of sequential trajectories in low score events (**Extended Data Fig. 2**). Thus, even events that would typically be classified as non-replays in POST maintain representations that are faithful to the maze place-fields.

While the stability and fidelity of spatial tunings were significantly greater in POST, these features did not last indefinitely. In our data that involved multiple hours of POST, we observed decreases in both the fidelity and stability of Bayesian learned tunings over the course of sleep (**Fig. 4a-c**). The similarity of sleep representations to maze place-fields decreased progressively over POST, eventually reaching levels similar to PRE. The stability of spatial tunings also decreased over this period, indicating that these representations become unreliable in later periods of sleep. The dissolution of representational alignment with the maze over the course of sleep may reflect an additional important aspect of sleep, distinct from that of reactivation and replay [21,22].

Retuning of representations during sharp-wave ripples in sleep

Recent studies report that place fields drift and frequently remap upon repeat exposures to the same environment [9,10,13,16,23] though it is unclear when and how these representational changes emerge. Given that the tunings learned during POST ripples display a diversity of place-field fidelities, some aligned but others misaligned with maze PFs, we asked whether these representations relate to the future spatial tunings of the cells. In three recording sessions from two animals, we re-exposed rats back to the maze environment after ~9 h of POST rest and sleep (**Fig. 5a**). We labelled these epochs "reMAZE" and compared the place fields across maze exposures with the ripple LTs from the intervening POST period (**Fig. 5b-d**). POST ripple LT's showed significant correlations with place fields from both maze exposures, indicating a continuity of representations across these periods. However, PFs were not identical between MAZE and reMAZE (**Fig. 5b**), illustrating that neuronal representations drift and remap in the rat hippocampus [10]. Consistent with our hypothesis that representational remapping emerging during POST could account for the deviations in PFs observed between repeated exposures to the maze, in instances where we saw reMAZE PFs congruent with MAZE PFs (top panel, **Fig. 5e**), the POST LTs for those cells showed strong fidelity with the maze period. However, in instances where reMAZE PFs deviated from the MAZE PFs (bottom panel, **Fig. 5e**), the POST LTs for those units predicted the PFs observed during maze reexposure. Likewise, we observed a significant correlation between PF fidelities in POST and the reMAZE-MAZE similarity (**Fig. 5f**) To better examine whether ripple representations during POST can presage representational changes across maze exposures, we performed a multiple regression analysis to test the extent to which reMAZE PFs are explained by MAZE PFs and LTs from PRE or POST (first 4 h). We also included the average LTs (over PRE and POST) to control for the general deviations of LTs that were not specific to any unit (**Fig. 5g**). This regression demonstrated a significant contribution (beta coefficient) for MAZE PFs, as expected, indicating that there is significant continuity in place-fields across maze exposures. However, it also revealed that POST LTs, but not PRE LTs, impact the PF locations in maze reexposure. Remarkably, when we repeated this analysis for last 4 hours of POST prior to reMAZE, we found no significant contribution from the late POST LTs (**Fig. 5h**), indicating that our observations do not simply arise from temporal proximity between POST sleep and the maze reexposure, but rather reflect rapid changes in representations that are manifested in the initial hours of sleep. Overall, these results demonstrate the critical role of POST sleep in stabilizing and reconfiguring the spatial representations of hippocampal neurons across exposures to an environment.

Sleep representations are driven by awake ripples and theta oscillations.

Our findings thus far indicate that the neuronal firing patterns during POST ripples reflect and retune the place-field representations on the maze. We next investigated the factors that conspire to establish these patterns. One recent study [24] reported that, more so than place field activity, the spike patterns of neurons during waking theta oscillations provide the necessary conditions for establishing the firing patterns observed during POST sleep. Another study, however, indicated that waking ripples are a primary mechanistic candidate for generating stable representations [25]. Adding further complication, several studies have indicated that PRE and POST ripples share overlapping activity structure [12,26], suggesting limits on the flexibility of sleep representations. To better understand the respective contributions of these different factors on the representations in POST sleep, we performed a multiple regression to test the extent to which POST LTs are explained by: PRE LTs, MAZE PFs, LTs of MAZE theta periods, and LTs of MAZE ripples (**Fig. 6a**). Remarkably, we found that the beta coefficients for all of

these regressors were significant. While the beta coefficient for MAZE theta LTs was significant, indicating that waking theta oscillations are important for the formation of ensemble representations, in support of the previous report [24], MAZE ripple LTs had the largest beta coefficient, indicating that firing patterns during waking ripples on the maze have the most lasting impact on POST sleep activity. Surprisingly, the second largest beta coefficients were observed for PRE ripple LTs, indicating that next to MAZE patterns, patterns configured in PRE also provide an important determinant of POST sleep activity [26,27]. Consistent with this, we observed a significant correlation between the PF fidelity in PRE and the PF fidelity in POST (**Fig. 6b**).

These observations suggest that despite the absence of maze tuning in PRE sleep, some cells maintain similar representations between PRE and POST. Sleep similarity, which measures the consistency of LTs across PRE and POST by assessing the correlation between PRE LTs and POST LTs, was significantly correlated with PF fidelity in PRE (**Fig. 6c**); thus, PRE LT's that aligned with maze PFs, presumably by chance, maintained those LTs in POST (see also individual examples in **Extended Data Fig. 1**, e.g. in Rat N). On the other hand, sleep similarity showed only a weak negative correlation with the PF fidelity in POST. To better understand the difference between PRE and POST LTs, we separated units into "PRE-tuned" cells (PRE PF fidelity > 0), and "PRE-untuned" cells (PRE PF fidelity < 0). PRE-tuned cells showed generally high POST PF fidelity along with high sleep similarity (**Fig. 6e**). In contrast, PRE-untuned cells showed a significant negative correlation between sleep similarity and POST fidelity (**Fig. 6f**); those with high sleep similarity were poorly tuned in POST, while those that reconfigured from PRE to POST, showed better fidelity to maze PFs. These analyses therefore reveal the contribution of PRE sleep to maze representations and POST activities; cells whose representations are already aligned with maze place fields in PRE maintain those same representations in POST, but other neurons display a broad range of flexible reconfiguration that is inversely proportional to their rigidity [27] across PRE and POST.

Discussion

The observations of dynamic representations in offline states made possible by Bayesian learning have important implications for our understanding of how learning and sleep impact the place-field representations of hippocampal neurons. First, we found that spatial representations emerge rapidly upon exposure to a novel environment, but not beforehand. While ripple events during pre-exposure occasionally scored highly for replays, spatial representations were not coherent among active neurons during these periods, as cells with very divergent place fields often fire within the same time bins (**Extended Data Fig. 2**). These observations suggest that continuous patterns in the decoded posteriors of spike trains could emerge spuriously. Consistent with this notion, it has been noted that the measures and shuffles used to quantify replays inevitably introduce unsupported assumptions about the nature of spontaneous activity [28-31]. We propose that only for those periods and events in which there is strong correspondence between the Bayesian learned tunings and neurons' place-fields, can the collective ensemble activity be considered to provide trajectories through internally generated representations of space [29,32].

Among the brain states we examined, sharp-wave ripples in early sleep offered the representations that best aligned with the place fields on the maze. These early sleep representations emerged from a confluence of factors, including carryover of firing patterns from pre-maze sleep (in both PRE-tuned and

PRE-untuned units)[30]. Most notably, however, our analysis revealed a key role in awake activity patterns during theta oscillations, and more prominently, those during sharp-wave ripples in generating the ensemble coordination that underlies spatial representations during sleep. These observations are consistent with the hypothesis that an initial cognitive map of space is first laid down during theta oscillations [18,24,33], then stabilized and continuously updated by awake replays based on the animal's (rewarded and/or aversive) experiences on the maze [25,32,34-36]. Once ensembles are established, they reactivate during early part of sleep [12,37]. However, sleep representations were not always exact mirror images of the maze place-fields, and our Bayesian learning approach allowed us to measure those deviations for individual neurons. Remarkably, we found that these early-sleep ripple representations proved predictive of place fields on re-exposure to the maze. Based on these observations, we propose that representational drift in fact arises rapidly from retuning that takes place during early sleep sharp-wave ripples rather than noisy deviations that develop spontaneously over time. Furthermore, we conjecture that hippocampal reactivations during sleep does not play a passive role in simply recapitulating the patterns already seen during learning but represents a key optimization process generating and integrating new spatial tunings within the recently formed spatial maps.

Overall, representations remained stable and consistent with the maze for hours of sleep in POST, despite the absence of strong sequential replay trajectories during ripples in POST sleep. Reconciling observations based on studies that measure neuronal reactivation using pairwise or ensemble measures with those that focus on trajectory replays has until now represented a challenge to the field [38]. Our study consolidates these views by demonstrating that faithful representations, which are consistent with pairwise and ensembles measures of reactivation, persist for hour-long durations. However, the trajectories produced by these cell ensembles do not necessarily provide continuous high-momentum sweeps through the maze environment [39,40], as we found high fidelity spatial tunings even among low replay score ripple events in post-maze sleep. Instead, trajectories simulated by the hippocampus during sleep ripples may explore pathways that were not directly experienced during waking but can serve to better consolidate a cognitive map of space. Additionally, we found increasing instability and drift in the spatial representations of neurons over the course of sleep, indicating that late sleep, like PRE, features more randomized activity patterns [21,41]. It is also worth noting that we did not find alignment between maze place fields and learned spatial tunings during REM sleep. It may be that under a different behavioral paradigm such as with frequently repeated maze exposures[42] or salient fear memories [43], or limiting analyses to specific phases of theta [44], we might have uncovered tunings more consistent with dream-like replays of maze place-fields [45]. On the other hand, it is also worth noting that the bulk of dreams do not reprise awake experiences [46]. The randomization of representations, as we see during REM and late stages of slow-wave sleep, may reflect an important function of sleep, driving activity patterns from highly-correlated ensembles to those with greater independence [22,47], which may be important for resetting the brain in preparation for new experiences [11].

In sum, the Bayesian learning approach provides a powerful means of tracking the stability and plasticity of representational tuning curves of neurons over time, which provides significant insights into how ensembles patterns form and reconfigure during offline state. A similar approach can be readily extended to investigate the dynamics of internally-generated representations in other neural systems during both sleep and awake states, including within rehearsal, rumination, or episodic simulation [48].

Figure Legends

Fig.1. Bayesian learning of hippocampal spatial tunings during offline states. (**a**) Hippocampal place cells show tuning to specific locations (place fields) on a linear track maze. When animals sleep or rest outside of the maze, the spiking of these neurons is no longer driven by maze location but may represent an internally generated simulation of x or another location. (**b**) We employed Bayesian learning to assess each neuron's tuning $p'(spike|x)$ for internally generated cognitive space, x, using the place fields of all other neurons recorded on the maze, under the assumption of conditional independence among Poisson spiking neurons conditioned on space. Top left, sample spike raster during an example maze traversal. Top right, spiking patterns of the same cells during a brief window in sleep. For each iteration, one cell is selected as the learning neuron. Bottom, left to right, population activity extracted for time bins in which the learning neuron spikes. Next, posterior probability distributions are constructed using the spikes and track tunings of the other neurons during these time-bins. The Bayesian learned tuning $p'(spike|x)$ is set to the summation of the posterior distributions over these time-bins ($\sum p(x|spike)$), normalized by the overall likelihood of each track location ($\sum p(x)$) obtained across the entire offline period.

Fig. 2. Bayesian learned tunings during MAZE and offline states. (**a**) Place fields (PFs) of hippocampal units pooled across sessions (814 units from 13 sessions and 10 rats) alongside Bayesian learned tunings (LTs) calculated separately for each behavioral epoch (PRE, MAZE, POST) and brain state (ripples, non-ripple NREM, REM, and active home cage). Only tunings learned during ripples on the MAZE and POST bear a visual resemblance to place fields. (**b**) The LT-PF correlations of the population vectors across space calculated between place fields and each set of learned tunings in (a). (**c**) Cumulative distributions of PF fidelity for each set of LTs in (a), defined as Pearson correlation coefficients between the LTs and PFs (r(LT, PF))**.** Only tunings learned during ripples on the MAZE and POST, along with non-ripple NREM, were significant compared to null distributions from 10000 unit identity shuffles (PRE; ripples: $p = 0.83$; non-ripple NREM: $p = 0.57$; REM: $p = 0.67$; active home cage: $p = 0.71$; MAZE; theta: $p < 10^{-4}$; ripples: $p < 10^{-4}$; POST; ripples: $p < 10^{-4}$; non-ripple NREM: $p = 2\times10^{-4}$; REM: $p = 0.72$; active home cage: $p = 0.11$). ** $p < 0.01$, *** $p < 0.001$.

Fig. 3. Stability of learned tunings during ripples in PRE and POST. (**a**) Heat maps of ripple LTs for sample units in sliding 15 min windows throughout a sample session from PRE through MAZE to POST (maze PFs in gray on right) show generally stable LTs during POST. Interestingly, units 5 and 6 also show stable tunings during PRE ripples, but those tunings do not align well with their maze place fields. (**b**) The matrix of correlation coefficients between LTs from different time windows for the units in (a) illustrate periods of stability. (**c**) Stability of the LTs (black) for the units in (a) in PRE and POST, defined as the median of the correlation coefficient between LTs from non-overlapping 15-min windows. Violin plots (gray) show the chance distributions obtained from non-identical units randomly scrambled across windows (1000x). While LTs of units 5 and 6 were stable within PRE and POST, they were not consistent across these epochs. (**d** and **e**) Unit LT stabilities z-scored against unit ID shuffles were significantly > 0 for the sample session (**d**) (PRE: median = 3.05, $p < 10^{-4}$; POST: median = 12.59, $p < 10^{-4}$; PRE-POST: median = 0.58, $p = 0.02$, WSRT ($n = 84$)) with individual units shown as dots, and (**e**) all sessions pooled together (PRE: median = 2.50, $p < 10^{-4}$; POST: median 4.68, $p < 10^{-4}$; across PRE w/ POST median = 0.66,

$p < 10^{-4}$, WSRT (n = 682 units)). However, LT stability in POST was higher than for both PRE or PRE w/ POST ($p < 10^{-4}$, WSRT (n = 682)). (**f**) Distributions of PF fidelity (r(LT, PF)) for units with stable (z > 2) versus unstable (z < 2) LTs showed no difference in PRE but were higher for stable units in POST ($p < 10^{-4}$, MWUT (n = 682)). ***P < 0.001; ns, not significant.

Fig. 4. Spatial representations are randomized over the course of sleep. (**a**) Heat maps of ripple LTs for sample units in sliding 15 min windows throughout a sample long duration session show gradual decreases in LT stability over time. A matrix of correlation coefficients between LTs from different time windows is provided on the right for each unit. (**b**) PF fidelity (correlation coefficient between LTs and PFs) shows a gradual decrease over time in POST. The color traces show median values across units within each individual session. The black trace and gray shade depict the median and interquartile range of the pooled data. PRE and MAZE epochs of differing durations were aligned to the onset of MAZE while POST epochs were aligned to the end of MAZE. (**c**) Left panels show LT stability correlation matrices averaged over all recorded units, shown separately for each dataset. Here, the matrix for each unit was z-scored against unit-ID shuffles prior to averaging. Right panels show the distribution of z-scored LT stability in overlapping 2-hour blocks during POST, separately for each dataset. The asterisks above each block represent the p-value of difference in LT stability compared with the previous block. *p < 0.05, ***p < 0.001.

Fig. 5. POST ripple tunings predict future place fields on maze re-exposure. (**a**)Timeline for sessions (n=3) in which the animal was re-exposed to the same maze track (reMAZE) after > 9 h from initial exposure (MAZE). We used the first 4 h of POST to calculate LTs. (**b**) Cumulative distribution of PF similarity between MAZE and reMAZE. (**c**) Cumulative distribution of POST PF fidelity (correlation coefficient between POST LTs and MAZE PFs). (**d**) Cumulative distribution of correlation coefficient between POST LTs and reMAZE PFs. (**e**) Example units with high MAZE/reMAZE similarity and high POST PF fidelity (top row), or low MAZE/reMAZE similarity and low POST PF fidelity (bottom row). The rightmost column shows the degree of similarity between the reMAZE PFs and POST LTs for each unit. (**f**) MAZE/reMAZE similarity correlated with POST PF fidelity. (**g**) Multiple regression analysis for modeling reMAZE PFs using PRE LTs, MAZE PFs, and POST LTs as regressors (RMSE = 0.91, $R^2 = 0.17$, $p < 10^{-4}$, $c_0 = 1.9\times10^{-16}$, $c_1 = 0.12$, $\beta_1 = -0.004$, p = 0.50, $\beta_2 = 0.25$, $p < 10^{-4}$, $\beta_3 = 0.15$, $p < 10^{-4}$; p-values against surrogate distributions from 10000 unit-identity shuffles of reMAZE PFs). (**h**) Same as (g) but using late POST (last 4 h) instead of POST LTs as a regressor (RMSE = 0.92, $R^2 = 0.16$, $p < 10^{-4}$, $c_0 = 2.6\times10^{-16}$, $c_1 = 0.16$, $\beta_1 = 0.04$, p = 0.10, $\beta_2 = 0.28$, $p < 10^{-4}$, $\beta_3 = 0.03$, p = 0.13).

Fig. 6. Ensemble patterns during awake theta and ripples and a diversity of pre-existing representations impact the tunings in POST sleep. (**a**) Multiple regression analysis for estimating the dependence of POST LTs on PRE LTs, MAZE PFs, MAZE theta LTs, and MAZE ripple LTs shows that POST LTs were most significantly impacted by PRE LTs and MAZE ripple LTs (RMSE = 0.75, $R^2 = 0.43$, $p < 10^{-4}$, $c_0 = -0.0002$, $c_1 = 0.15$, $\beta_1 = 0.27$, $p < 10^{-4}$, $\beta_2 = 0.07$, $p < 10^{-4}$, $\beta_3 = 0.15$, $p < 10^{-4}$, $\beta_4 = 0.30$, $p < 10^{-4}$, p-values against surrogate distributions from 10000 unit-identity shuffles). (**b**) PF fidelity (correlation with MAZE PF) was significantly correlated between PRE and POST LTs. (**c**) Sleep similarity (correlation between PRE and POST LTs) was correlated with PRE PF fidelity, indicating that high fidelity PRE LTs are preserved in POST. (**d**) An overall weak negative correlation between sleep similarity and POST PF fidelity. When we

split units into PRE-tuned (PRE PF fidelity > 0) and PRE-untuned PFs (PRE PF fidelity < 0)**,** (**e**) there was little correlation between sleep similarity and POST fidelity for PRE-tuned cells. (**f**) For PRE-untuned cells, a negative correlation between POST PF fidelity and sleep similarity indicates a continuum of flexible retuning to maze PF.

Methods

Behavioral task and data acquisition. We trained four water-deprived rats to alternate between two water wells in a previously habituated home box. Water rewards during the alternation were delivered via water pumps interfaced with custom-built Arduino hardware. After the animals learned the alternation task, they were surgically implanted under deep isoflurane anesthesia with 128 channel silicon probes (8 shanks, Diagnostic Biochips, Glen Burnie, MD) either unilaterally (one rat) or bilaterally (three rats) over the dorsal hippocampal CA1 subregions (AP:-3.36 mm , ML:$\pm$ 2.2 mm). Following recovery from surgery, the probes were gradually lowered over a week to the CA1 pyramidal layer, which was identified by sharp wave-ripple polarity reversals and frequent neuronal firing. After ensuring recording stability, the animals were exposed to novel linear tracks during one (three rats) or two (one rat) behavioral sessions (in total five sessions from the four rats). During each session, the implanted animal was first placed in the home box (PRE, ~ 3 hours) with ad libitum sleep (during the dark cycle). Then, the animal was transferred to a novel linear track with two water wells that were mounted on platforms at either end of the track (MAZE, ~ 1 hour). After running on the linear track for multiple laps for water rewards, the animal was returned to the home box (aligned with the start of the light cycle) for another ~10 hours of ad libitum sleep (POST). In four of these sessions, following POST the rats were re-exposed to the same linear track for another ~ 1h of running for reward (reMAZE).

Wideband extracellular signals were recorded at 30 kHz using an OpenEphys board [49] or an Intan RHD recording controller during each session. The wideband activity was high-pass filtered with a cut-off frequency of 500 Hz and thresholded at five standard deviations above the mean to extract putative spikes. The extracted spikes were first sorted automatically using SpykingCircus [50], followed by a manual passthrough using Phy [51] (https://github.com/cortex-lab/phy/). Only units with less than 1% of total number of spikes in their refractory period (based on the units' autocorrelograms) were included in further analysis. Putative neurons were classified into pyramidal and interneurons based on peak waveform shape, firing rate, and interspike intervals [52,53]. For analysis of local field potentials (LFP, 0.5-600 Hz), signals were filtered and downsampled to 1250 Hz.

The animal's position was tracked using an Optitrack infrared camera system (NaturalPoint Inc, Corvalis, OR) with infrared-reflective markers mounted on a plastic rigid body that was secured to the recording headstage. 3D position data was extracted online using Motive software (Optitrack), sampled at either 60 Hz or 120 Hz, and later interpolated for aligning with the ephys data. Although, we attempted to track the animal's position during each entire session, including in the home cage, the cage limited visual access from our fixed cameras. Additionally, in one session the position data for reMAZE was lost during the recording.

These data comprised the Giri dataset used in our study. We also took advantage of previously published data described in detail in a previous report [12]. This data consisted of recordings of unit and local field potential from the rat hippocampus CA1 region, with PRE rest and sleep, exposure to a novel MAZE, and POST rest and sleep: the Miyawaki dataset (3 rats, 5 sessions; PRE, MAZE, POST, each ~ 3 hours)[12,21] and the Grosmark dataset (4 rats, 5 sessions; PRE, and POST, each ~ 4 hours and MAZE, ~ 45 minutes)[27]. See Supplementary Table 1 for further details of each session. These data are available upon request from the corresponding author. Custom-written MATLAB code supporting this study is available at https://github.com/diba-lab/Maboudi_et_al_2022. All animal procedures followed protocols approved by the Institutional Animal Care and Use Committees (IACUC) at the University of Wisconsin-

Milwaukee and the University of Michigan, and conformed to guidelines established by the United States National Institutes of Health.

Place field calculations. To calculate place fields, we first linearized the position by projecting each two-dimensional track position onto a line that best fit the average trajectories taken by the animal over all traversals within each session. The entire span of the linearized position was divided into 2 cm position bins and the spatial tuning curve of each unit was calculated as occupancy-normalized spike counts across the linearized position bins. With the exception of **Extended Data Fig. 1**, only units with place fields that had a peak firing rate > 1 Hz were included.

Local field potential analysis and brain state detection. We estimated a broadband slow wave metric using the irregular-resampling auto-spectral analysis (IRASA) approach [54], following code generously shared by Dan Levenstein and the Buzsaki lab (https://github.com/buzsakilab/buzcode). This procedure allows estimation of the slope of the power spectrum which is used to estimate slow-wave activity. The slow-wave metric for each session followed a bimodal distribution with a dip that provided a threshold to distinguish NREM (non "rapid eye movement" sleep) from other periods. A time-frequency map of the local field potential (LFP) was also calculated in sliding 1s windows, step size of 0.25 s, using the Chronux toolbox [55]. To identify high theta periods, such as during active waking or REM sleep [21,56], the theta/non-theta ratio was estimated at each time point as the ratio of power in theta (4-9 Hz in home cage and 6-11 Hz on the linear track) to a summation of power in delta frequency band (1-4 Hz) and the frequency gap between the first and second harmonics of theta (10-12 Hz during home cage awake and REM epochs and 11–15 Hz during MAZE). To calculate the ripple power, multichannel LFP signals were filtered in the range of 150-250 Hz. The envelope of the ripple LFP was calculated using the Hilbert transform, z-scored and averaged across the channels. Only channels with the highest ripple power from each electrode shank were used in the averaging.

Detection of ripple events. For each recording session, multi-unit firing rates (MUA) were calculated by binning the spikes across all recorded single units and multi-units in 1 ms time bins. Smoothed MUA was obtained by convolving the MUA with a Gaussian kernel with $\sigma = 10\ ms$ and z-scoring against the distribution of firing rates over the entire session. Ripple events were first marked by increased MUA firing, periods when the smoothed MUA crossed 2z and the boundaries were extended to the nearest zero-crossing time points. The ripple events that satisfied the following criteria were considered for further analysis: a) duration between 40 and 600 milliseconds, b) occurrence during NREM or quiet waking period, c) concurrent speed of the animal below 10 cm/sec (when available), and d) concurrent ripple power in the LFP higher than 1 s.d. above the mean. To detect the ripple events during the quiet waking periods, we required either a theta-delta ratio < 1 or ripple power > 3 s.d. of the mean at the time of candidate event. All ripple events were subsequently divided into 20 millisecond time bins. The onsets and offsets of the events were adjusted to first time bins with at least two pyramidal units firing. We split ripples with silent periods > 40 ms into two or more events.

Bayesian learned tunings. Bayesian learning of spatial tunings or learned tunings (LTs) can be conceptualized as using offline spiking activity to update our estimate of each unit i's spatial tuning $p(s_i|x)$, which is the probability of spiking conditioned on the network's internal estimate of position, x. Outside of the maze, the best initial estimate available for a cell's place preferences is its place field on the maze. Then, Bayesian learning [15] is used to update this tuning curve based on information available in the spike trains from the epoch of interest. Note that this approach still relies on the place-fields of

neurons as measured on the maze. However, it provides a degree of separation in that a given neuron's Bayesian LT does not depend directly on its own maze place-field, but rather on the coherent firing of that neuron with the other neurons in the ensemble.

Effectively, the unit i's LT is learned from the posterior probability distributions $p(x|s_{\forall j\neq i})$ determined from the other units' spikes for the time windows in which unit i spikes. The posterior probability distribution, $p(x|s_{\forall j\neq i})$ within individual time bins is calculated based on other units, excluding the spikes and track tuning of unit i itself, under the assumption of conditional independence among hippocampal neurons conditioned on maze position and running direction.

Since majority of the sessions (16 out of 17) consisted of two running directions on the track, we first calculated the posterior joint probability of position and travel direction and then marginalized the joint probability distribution over travel direction [57]:

$$p(x,d|s_{\forall j\neq i}) \propto p(s_1,s_2,\dots,s_{i-1},s_{i+1},\dots,s_n\,|x,d) \quad (1)$$

in which n is the total number of units and d signifies the travel direction. With the assumption of independent Poisson-distributed firings of individual units conditioned on maze position and direction, equation (1) is equal to:

$$p(x,d|s_{\forall j\neq i}) \propto \prod_{j\neq i}(f_j(x,d)\,\tau)^{s_j}\, e^{-f_j(x,d)\,\tau} \quad (2)$$

In equation (2), $f_j(x,d)$ characterizes the mean firing rate of unit j at position bin x and direction d and τ is the bin duration used for decoding, which was chosen = 20 ms in our analyses. By marginalizing the left hand side of equation (2) over direction d:

$$p(x|s_{\forall j\neq i}) \propto \sum_d p(x,d|s_{\forall j\neq i}) \quad (3)$$

Then, the Bayesian learned tuning for unit i was calculated as:

$$p'(s_i|x) = \sum_k k * p(s_i = k|x) \quad (4)$$

in which

$$p(s_i = k|x) = p(x|s_{\forall j\neq i}\ \&\ s_i = k) * p(s_i = k)/p(x) \quad (5)$$

Where $p(x|s_{\forall j\neq i}\ \&\ s_i = k)$ is the average posterior probability of track position, x, over time bins in which the unit i fired k spikes, calculated using only units $\neq i$. $p(s_i = k)$ is the overall proportion of time bins where unit i fired k spikes, and $p(x)$ is average posterior over all time bins.

The equation (4) for calculating the LTs was simplified to the unit i's spike-triggered average of the posterior probability distributions:

$$p'(s_i|x) = \frac{\sum_t k_t * p_t(x|s_{\forall j\neq i})}{\sum_t p_t(x|s_{\forall j\neq i})} \quad (6)$$

in which t is the time bin and k_t is the number of spikes that unit i fired at t.

Additional restrictions to avoid potential confounds from unit waveform clustering: To avoid potential confounds from spike misclassification of units detected on the same shank [58], we placed additional

inclusion requirements for LT calculations. We determined the L-ratios [59] between unit i and each other unit recorded on the same shank, yielding the cumulative probability of the other units' spikes belonging to unit i. Since the range of L-ratio depends on the number of included channels, to provide a consistent threshold for all datasets, the L-ratio for each pair was calculated using the four channels that featured the highest spike amplitude difference between each pair of units. Only units with L-ratio > 10^{-3} (see **Extended Data Fig. 3**) were used to calculate LTs for each cell.

Fidelity of the learned tunings across epochs. To quantify the degree to which tuning curves, $p(x|s)$, in LTs or PFs relate across epochs, we used a simple Pearson correlation coefficient of the tuning curves across position bins between the LTs/PFs. We obtained consistent results with a measure based on the Kullback-Leibler divergence (not shown). The median for each epoch were compared against a surrogate distribution of such median values obtained by shuffling the unit identities of the PFs separately (10000 times) within each session. In other words, we tested against the null hypothesis that learned tunings in each session may have trivial correlations with PFs. For each epoch we obtained p-values based on the number of such surrogate median values that were ≥ those in the original data. With the exception of **Fig.2** only units that participated in > 100 ripple events in PRE or POST were included in the analysis.

Learned tuning's dynamics. We further evaluated the dynamics of LTs across time in non-overlapping 15 min windows (for illustration purposes only in **Fig. 3**, we used overlapping 15 min windows with a 5 min step size). A unit's LT stability was defined as the median Pearson correlation coefficient between that unit's LTs in all different pairs of time windows within a given epoch. Thus, units that had stable and consistent LTs across an epoch yield higher correlations in these comparisons than those with unstable LTs. These unit LT stability values were z-scored against a null distribution of median correlation coefficients based on randomizing the LTs' unit identities within each 15 min time window (1000 unit ID shuffles). Normalized stability correlation matrices in **Fig. 4c** were calculated by z-scoring each correlation coefficient against a surrogate distribution based on shuffling the LTs' unit identities. To investigate the changes in POST LT stability over time in **Fig. 4c**, we calculated LT stability within overlapping 2-hour blocks with a step size of one hour.

Ripple event replay scores. The posterior probability matrix (P) for each ripple event was calculated based on previously published methods. Replays were scored using the absolute weighted correlation between decoded position (x) and time bin (t) [31]:

$$corr(t,x;p) = \frac{cov(t,x;P)}{\sqrt{cov(t,t;P)cov(x,x;P)}} \quad (7)$$

$$cov(t,x;P) = \frac{\sum_i \sum_j P_{ij}(x_j - m(x;P))(t_i - m(t;P))}{\sum_i \sum_j P_{ij}} \quad (8)$$

$$m(x;P) = \frac{\sum_i \sum_j P_{ij} x_j}{\sum_i \sum_j P_{ij}} \qquad m(t;p) = \frac{\sum_i \sum_j P_{ij} t_i}{\sum_i \sum_j P_{ij}} \quad (9)$$

In which i and j index time bin and position bin, respectively.

Each replay score was further quantified as a percentile relative to surrogate distributions obtained by shuffling the data according to the commonly used within-event time swap, in which time bins are randomized within each ripple event [57]. We preferred this method over the circular spatial bin shuffle (or column cycle shuffle, also described by [57], as it preserves the distribution of peak locations across time bins within each event (see also related discussion in ref[30]). Each ripple event was assigned to one of four quartiles based on the percentile score of the corresponding replay relative to shuffles

Place fields' overlap with decoded posterior. A Pearson correlation coefficient was calculated between the PF of each unit firing (participating) in a time-bin and the posterior probability distribution for that bin based on the firings of all units. The mean posterior correlation of PFs was calculated over all participating units. Since this mean posterior correlation might be inflated when there is a low number of participating units, for each time bin with firing unit count n we generated surrogate distribution of mean posterior correlation by randomly selecting n units. Then, the mean posterior correlation in the original data was z-scored against the corresponding surrogate distribution for n randomly participating units.

Multiple regression analyses. To examine the extent to which a spatial tuning curve (LT or PF) within a given epoch was impacted by the tuning curves in other epochs, we performed multiple regression analyses. We modeled POST LTs and reMAZE PFs using the following equations:

$$POST\ LTs = c_0 + c_1 * average\ LT + \beta_1 * PRE\ LTs + \beta_2 * MAZE\ PFs + \beta_3 * MAZE\ theta\ LTs + \beta_4 * MAZE\ ripple\ LTs \quad (9)$$

$$reMAZE\ PFs = c_0 + c_1 * average\ LT + \beta_1 * PRE\ LTs + \beta_2 * MAZE\ PFs + \beta_3 * POST\ LTs \quad (10)$$

The dependent variables and regressors were calculated over all position bins from all units. The average LT in the analyses were calculated by averaging all unit LTs over PRE and POST. cs and βs are the regression coefficients.

In order to test the statistical significance of the regression R^2 values and each regression β coefficient, we compared these against distributions of surrogates (n = 10,000) which were calculated by randomizing the unit identities of the dependent variable's tuning curves. For each coefficient and R^2 values, we obtained a p-value based on the number of surrogates that were $\geq$ those in the original data.

Supplementary Information

Representations during high score preplays do not align with maze place fields.

The sequential firing patterns observed during ripples in sleep show a diversity of faithfulness to trajectories through the maze, as captured in the distribution of replay (and preplay) scores (**Extended Data Fig. 3a**) in the datasets we analyzed using a commonly used weighted-correlation measure, advocated by several studies [27,30,31]. Here, each event was scored as a percentile compared to its own surrogate distributions generated using a within-ripple-event time-bin shuffle [57] (see **Methods**). These distributions varied from a uniform distribution expected from chance in all datasets (expected median replay score = 50), not only for MAZE, and POST epochs, but also for PRE, consistent with previous reports [27,30,60]. Replay scores during MAZE showed the greatest deviation from chance. While we expected more replay than preplay based on previous reports [27,30,31], POST and PRE replay scores were only marginally different in one out of the three datasets we examined (*Grosmark dataset*: PRE: median = 53.8, POST: median = 57.2, PRE vs POST $p = 3.45\times10^{-12}$, Mann Whitney U Test (MWUT); *Miyawaki dataset*: PRE: median = 50.8 , POST: median = 51.2, PRE vs POST p = 0.47, MWUT; *Giri dataset*: PRE: median = 56.6 , POST: median = 55.6, PRE vs POST p = 0.42, MWUT).

Since replays are considered to simulate trajectories through the maze, we asked whether tunings learned from higher score ripple events in either PRE or POST might show greater fidelity to the maze PFs. We therefore calculated LTs from four subsets of ripples events with replay scores of different percentiles (**Extended Data Fig. 2b,c**). We called the tunings learned from the lowest and highest quartiles "low score" and "high score" LTs, respectively. Remarkably, both the low score and high score LTs from MAZE and POST showed strong fidelity to maze PFs, despite the absence of sequential trajectories in low score events. In contrast, neither high nor low score LTs in PRE showed LTs consistent with the maze PFs (**Extended Data Fig. 2b**). LTs from all quartiles of replay scores showed significant PF fidelity in MAZE and POST but not in PRE (**Extended Data Fig. 2c**), with somewhat stronger PF fidelity in higher score quartiles (PRE: $\chi^2 = 7.2$, p = 0.07; MAZE: $\chi^2 = 143$, $p < 10^{-30}$; POST: $\chi^2 = 150.7$, $p < 10^{-31}$, Friedman test). Likewise, the spatial population vector correlations of low and high score LTs showed a strong correlation with maze PFs for both MAZE and POST epochs, but not for PRE. Overall, these results delineate that even during ripple events in POST with low replay scores, which are typically discarded as non-replays by most measures, the representational structures of neuronal spike trains remain congruent with the place fields on the maze. The firing patterns underlying these events could be detected as "reactivation" using pairwise or ensemble measures [12,38,61], but rather than providing a sequential sweep through space that would be necessary to score high for replay, such ripple events may provide non-continuous, low momentum, or random trajectories through the maze [39,40]. In contrast, however, even during ripple events in PRE that appear to show sequential structure, the neurons cannot be said to represent the same locations as they do on the maze.

To better understand the dichotomy between PRE and POST ripples, we examined the decoded posterior positions and unit rasters of individual ripple events with high replay scores. In high score ripple events in PRE (e.g. examples shown in **Extended Data Fig. 2d**), even though these events appeared to show sequential trajectories leading to high scores, we could not distinguish this sequential structure in the spike trains of units sorted according to their preferred maze locations (such structure

was evident in some high score events in POST, e.g. the second two panels). Inspection of individual bins revealed that units which were co-active in time-bins during PRE ripple events possessed highly divergent place fields with relatively low mean correlations with the collective posterior probability distributions, contrary to expectations from a unified population code. In contrast, the place fields of units in POST high and low score events showed a greater resemblance (and stronger mean correlation) with the posteriors in their respective bins, indicative of a coherent population representation. Mean posterior correlations of active PFs in bins during all ripple events in PRE and POST similarly showed no significant difference in between low and high score events in PRE, but they were significantly higher in POST relative to PRE (similar results were observed even when we restricted analysis to the subset of events that featured low jump distances (i.e. more continuous trajectories) between time bins (not shown)[30,31]). The shuffling methods employed to score replays in our and other studies invariably involve assumptions that are violated in real data [28-30]. These results highlight the importance of verification, as we propose via Bayesian learned tunings, to ensure that decoded positions are in fact consistent with representations of place fields on the maze.

Supplementary Table 1: summary of recording datasets

Dataset	**Animal ID**	**Sex**	**Maze type**	**Number of pyramidal units**
Giri	Rat N	F	L-shape	84
	Rat S	F	L-shape	78
	Rat U	M	Semicircular (reMAZE)	174
	Rat V	M	Linear (reMAZE)	47
			Semicircular (reMAZE)	78
				Total 461
Miyawaki	Rat R	M	Linear	84
	Rat T	M	Linear	58
			L-shape	41
			U-shape	78
	Rat K	M	Linear	62
				Total 323
Grosmark	Rat A	M	Linear	148
			Circular	101
	Rat B	M	Linear	57
	Rat C	M	Linear	53
	Rat G	M	Circular	52
				Total 411

Extended Data Figure Legends

Extended Data Figure 1. Additional examples that demonstrate the degree of LT stability within and between different behavioral epochs. Heat maps of ripple LTs in sliding 15 min windows from PRE through MAZE to POST (maze PFs in gray on right) for sample units from 5 additional sessions. The matrix of correlation coefficients between LTs from different time windows are displayed next to the corresponding heat maps.

Extended Data Fig. 2. Place field fidelities do not strictly correlate with replay score. (**a**) Distribution of replay scores in the different datasets calculating as percentile against time shuffled bins. Median scores for different epochs are shown with dashed lines (chance median score = 50; see **Methods**). (**b**) Ripple events were divided into quartiles according to replay score. Top panels show the place fields and sets of LTs calculated based on low and high quartile replay score events within PRE, MAZE, and POST. Bottom panels show population vector (PV) correlations between position bins in the PFs versus different sets of LTs. (**c**) Distribution of PF fidelity for each ripple subset. Median PF fidelities were significant against surrogate distributions (from unit identity shuffles) in all subsets during MAZE and POST but not during PRE. (**d**) Place fields of participating units in replays show differing amounts of overlap with the decoded posteriors. Example events with high replay scores in PRE and POST, and low replay scores in POST showing posterior probability matrices and corresponding spike rasters of units sorted by place field order. The middle row depicts the mean correlation of the participating units' place fields with the decoding posterior in each time bin. The bottom panels show the place fields and decoded positions of participating units for example time bins. (**e**) Mean posterior correlation of PFs and decoded positions show increased place-field overlap in both low and high score replays in POST compared to PRE. Low and high replay score events in PRE did not differ significantly. ***$p < 0.001$.

Extended Data Figure 3. A L-ratio measure to quantify the degree of overlap in the spike feature space between pairs of units. (**a**) Each scatterplot on the top shows the spikes of the example unit #20 (black dots) and another unit (colored dots) recorded on the same shank in an example recording session from the Giri dataset. The axes in each scatterplot correspond to the spike amplitude on two channels with maximal distinction between the pairs. There is a range of overlap with unit #20; for example, unit #30 on the leftmost inset showed almost no overlap, while unit 19 on the rightmost inset significantly overlapped. The overlap was quantified as an L-ratio on the top of each inset. The L-ratio between unit #20 and any other unit was obtained by calculating the probability of spikes from the second unit belonging to unit 20. The insets on the second row show the comparison between the mean spike amplitudes for each unit pair as plotted in the scatterplots. (**b**), The cumulative distribution of L-ratio for the example session and pooled data across all sessions (left), and for each individual session (right).

References

1. Klinzing, J.G., Niethard, N. & Born, J. Mechanisms of systems memory consolidation during sleep. *Nat Neurosci* **22**, 1598-1610 (2019).
2. Havekes, R. & Abel, T. The tired hippocampus: the molecular impact of sleep deprivation on hippocampal function. *Curr Opin Neurobiol* **44**, 13-19 (2017).
3. Hebb, D.O. *The organization of behavior*, (Wiley, New York, NY, 1949).
4. O'Keefe, J. & Dostrovsky, J. The hippocampus as a spatial map. Preliminary evidence from unit activity in the freely-moving rat. *Brain Res* **34**, 171-175 (1971).
5. Zhang, K., Ginzburg, I., McNaughton, B.L. & Sejnowski, T.J. Interpreting neuronal population activity by reconstruction: unified framework with application to hippocampal place cells. *J Neurophysiol* **79**, 1017-1044 (1998).
6. Frank, L.M., Stanley, G.B. & Brown, E.N. Hippocampal plasticity across multiple days of exposure to novel environments. *J Neurosci* **24**, 7681-7689 (2004).
7. Dong, C., Madar, A.D. & Sheffield, M.E.J. Distinct place cell dynamics in CA1 and CA3 encode experience in new environments. *Nat Commun* **12**, 2977 (2021).
8. Alme, C.B.*, et al.* Place cells in the hippocampus: eleven maps for eleven rooms. *Proc Natl Acad Sci U S A* **111**, 18428-18435 (2014).
9. Ziv, Y.*, et al.* Long-term dynamics of CA1 hippocampal place codes. *Nat Neurosci* **16**, 264-266 (2013).
10. Mankin, E.A.*, et al.* Neuronal code for extended time in the hippocampus. *PNAS* **109**, 19462-19467 (2012).
11. Cirelli, C. & Tononi, G. The why and how of sleep-dependent synaptic down-selection. *Semin Cell Dev Biol* **125**, 91-100 (2022).
12. Giri, B., Miyawaki, H., Mizuseki, K., Cheng, S. & Diba, K. Hippocampal Reactivation Extends for Several Hours Following Novel Experience. *J Neurosci* **39**, 866-875 (2019).
13. Grosmark, A.D., Sparks, F.T., Davis, M.J. & Losonczy, A. Reactivation predicts the consolidation of unbiased long-term cognitive maps. *Nat Neurosci* **24**, 1574-1585 (2021).
14. Pettit, N.L., Yap, E.L., Greenberg, M.E. & Harvey, C.D. Fos ensembles encode and shape stable spatial maps in the hippocampus. *Nature* **609**, 327-334 (2022).
15. Wiskott, L. Lecture Notes on Bayesian Theory and Graphical Models. (2013).
16. Rule, M.E., O'Leary, T. & Harvey, C.D. Causes and consequences of representational drift. *Curr Opin Neurobiol* **58**, 141-147 (2019).
17. Diba, K. & Buzsaki, G. Forward and reverse hippocampal place-cell sequences during ripples. *Nat Neurosci* **10**, 1241-1242 (2007).
18. Dragoi, G. & Buzsaki, G. Temporal encoding of place sequences by hippocampal cell assemblies. *Neuron* **50**, 145-157 (2006).
19. Siclari, F.*, et al.* The neural correlates of dreaming. *Nat Neurosci* **20**, 872-878 (2017).
20. Vertes, R.P. & Eastman, K.E. The case against memory consolidation in REM sleep. *Behav Brain Sci* **23**, 867-876; discussion 904-1121 (2000).
21. Miyawaki, H. & Diba, K. Regulation of Hippocampal Firing by Network Oscillations during Sleep. *Curr Biol* **26**, 893-902 (2016).
22. Norimoto, H.*, et al.* Hippocampal ripples down-regulate synapses. *Science* **359**, 1524-1527 (2018).
23. Kinsky, N.R., Sullivan, D.W., Mau, W., Hasselmo, M.E. & Eichenbaum, H.B. Hippocampal Place Fields Maintain a Coherent and Flexible Map across Long Timescales. *Curr Biol* **28**, 3578-3588 e3576 (2018).

24. Drieu, C., Todorova, R. & Zugaro, M. Nested sequences of hippocampal assemblies during behavior support subsequent sleep replay. *Science* **362**, 675-679 (2018).
25. Roux, L., Hu, B., Eichler, R., Stark, E. & Buzsaki, G. Sharp wave ripples during learning stabilize the hippocampal spatial map. *Nat Neurosci* **20**, 845-853 (2017).
26. Liu, K., Sibille, J. & Dragoi, G. Preconfigured patterns are the primary driver of offline multi-neuronal sequence replay. *Hippocampus* **29**, 275-283 (2019).
27. Grosmark, A.D. & Buzsaki, G. Diversity in neural firing dynamics supports both rigid and learned hippocampal sequences. *Science* **351**, 1440-1443 (2016).
28. Foster, D.J. Replay Comes of Age. *Annu Rev Neurosci* **40**, 581-602 (2017).
29. van der Meer, M.A.A., Kemere, C. & Diba, K. Progress and issues in second-order analysis of hippocampal replay. *Philos Trans R Soc Lond B Biol Sci* **375**, 20190238 (2020).
30. Farooq, U., Sibille, J., Liu, K. & Dragoi, G. Strengthened Temporal Coordination within Pre-existing Sequential Cell Assemblies Supports Trajectory Replay. *Neuron* **103**, 719-733 e717 (2019).
31. Silva, D., Feng, T. & Foster, D.J. Trajectory events across hippocampal place cells require previous experience. *Nat Neurosci* **18**, 1772-1779 (2015).
32. Diba, K. Hippocampal sharp-wave ripples in cognitive map maintenance versus episodic simulation. *Neuron* **109**, 3071-3074 (2021).
33. Monaco, J.D., Rao, G., Roth, E.D. & Knierim, J.J. Attentive scanning behavior drives one-trial potentiation of hippocampal place fields. *Nat Neurosci* **17**, 725-731 (2014).
34. Gupta, A.S., van der Meer, M.A., Touretzky, D.S. & Redish, A.D. Hippocampal replay is not a simple function of experience. *Neuron* **65**, 695-705 (2010).
35. Mattar, M.G. & Daw, N.D. Prioritized memory access explains planning and hippocampal replay. *Nat Neurosci* **21**, 1609-1617 (2018).
36. Cheng, S. & Frank, L.M. New experiences enhance coordinated neural activity in the hippocampus. *Neuron* **57**, 303-313 (2008).
37. Wilson, M.A. & McNaughton, B.L. Reactivation of hippocampal ensemble memories during sleep. *Science* **265**, 676-679 (1994).
38. Tingley, D. & Peyrache, A. On the methods for reactivation and replay analysis. *Philos Trans R Soc Lond B Biol Sci* **375**, 20190231 (2020).
39. Krause, E.L. & Drugowitsch, J. A large majority of awake hippocampal sharp-wave ripples feature spatial trajectories with momentum. *Neuron* **110**, 722-733 e728 (2022).
40. Stella, F., Baracskay, P., O'Neill, J. & Csicsvari, J. Hippocampal Reactivation of Random Trajectories Resembling Brownian Diffusion. *Neuron* **102**, 450-461 e457 (2019).
41. Genzel, L., Kroes, M.C., Dresler, M. & Battaglia, F.P. Light sleep versus slow wave sleep in memory consolidation: a question of global versus local processes? *Trends Neurosci* **37**, 10-19 (2014).
42. Louie, K. & Wilson, M.A. Temporally structured replay of awake hippocampal ensemble activity during rapid eye movement sleep. *Neuron* **29**, 145-156 (2001).
43. Boyce, R., Glasgow, S.D., Williams, S. & Adamantidis, A. Causal evidence for the role of REM sleep theta rhythm in contextual memory consolidation. *Science* **352**, 812-816 (2016).
44. Poe, G.R., Nitz, D.A., McNaughton, B.L. & Barnes, C.A. Experience-dependent phase-reversal of hippocampal neuron firing during REM sleep. *Brain Res* **855**, 176-180 (2000).
45. Hobson, J.A. REM sleep and dreaming: towards a theory of protoconsciousness. *Nat Rev Neurosci* **10**, 803-813 (2009).
46. Vertes, R.P. Memory consolidation in sleep; dream or reality. *Neuron* **44**, 135-148 (2004).
47. Colgin, L.L., Kubota, D., Jia, Y., Rex, C.S. & Lynch, G. Long-term potentiation is impaired in rat hippocampal slices that produce spontaneous sharp waves. *J Physiol* **558**, 953-961 (2004).

48. Schacter, D.L., Addis, D.R. & Buckner, R.L. Episodic simulation of future events: concepts, data, and applications. *Ann N Y Acad Sci* **1124**, 39-60 (2008).
49. Siegle, J.H.*, et al.* Open Ephys: an open-source, plugin-based platform for multichannel electrophysiology. *J Neural Eng* **14**, 045003 (2017).
50. Yger, P.*, et al.* A spike sorting toolbox for up to thousands of electrodes validated with ground truth recordings in vitro and in vivo. *eLife* **7**(2018).
51. Rossant, C.*, et al.* Spike sorting for large, dense electrode arrays. *Nat Neurosci* **19**, 634-641 (2016).
52. Bartho, P.*, et al.* Characterization of neocortical principal cells and interneurons by network interactions and extracellular features. *J Neurophysiol* **92**, 600-608 (2004).
53. Petersen, P.C., Siegle, J.H., Steinmetz, N.A., Mahallati, S. & Buzsaki, G. CellExplorer: A framework for visualizing and characterizing single neurons. *Neuron* **109**, 3594-3608 e3592 (2021).
54. Wen, H. & Liu, Z. Separating Fractal and Oscillatory Components in the Power Spectrum of Neurophysiological Signal. *Brain Topogr* **29**, 13-26 (2016).
55. Bokil, H., Andrews, P., Kulkarni, J.E., Mehta, S. & Mitra, P.P. Chronux: a platform for analyzing neural signals. *J Neurosci Methods* **192**, 146-151 (2010).
56. Buzsaki, G. Theta oscillations in the hippocampus. *Neuron* **33**, 325-340 (2002).
57. Davidson, T.J., Kloosterman, F. & Wilson, M.A. Hippocampal replay of extended experience. *Neuron* **63**, 497-507 (2009).
58. Quirk, M.C. & Wilson, M.A. Interaction between spike waveform classification and temporal sequence detection. *J Neurosci Methods* **94**, 41-52 (1999).
59. Schmitzer-Torbert, N., Jackson, J., Henze, D., Harris, K. & Redish, A.D. Quantitative measures of cluster quality for use in extracellular recordings. *Neuroscience* **131**, 1-11 (2005).
60. Dragoi, G. & Tonegawa, S. Preplay of future place cell sequences by hippocampal cellular assemblies. *Nature* **469**, 397-401 (2011).
61. Kudrimoti, H.S., Barnes, C.A. & McNaughton, B.L. Reactivation of hippocampal cell assemblies: effects of behavioral state, experience, and EEG dynamics. *J Neurosci* **19**, 4090-4101 (1999).

Acknowledgements

We thank Ted Abel, George Mashour, Asohan Amarasingham, Matthijs van der Meer, Nat Kinsky, Pho Hale, and Rachel Wahlberg for valuable comments on the manuscript. This work was funded by NINDS R01NS115233 and NIMH R01MH117964.

Author Contributions

KD and KM conceived the analytical approach. BG conceived and performed reMAZE and sleep experiments. HM performed maze/sleep recordings. KM performed all analyses. KD supervised the research with input from CK. KD and KM wrote the manuscript with feedback from CK and HM.

Figures

Figure 1

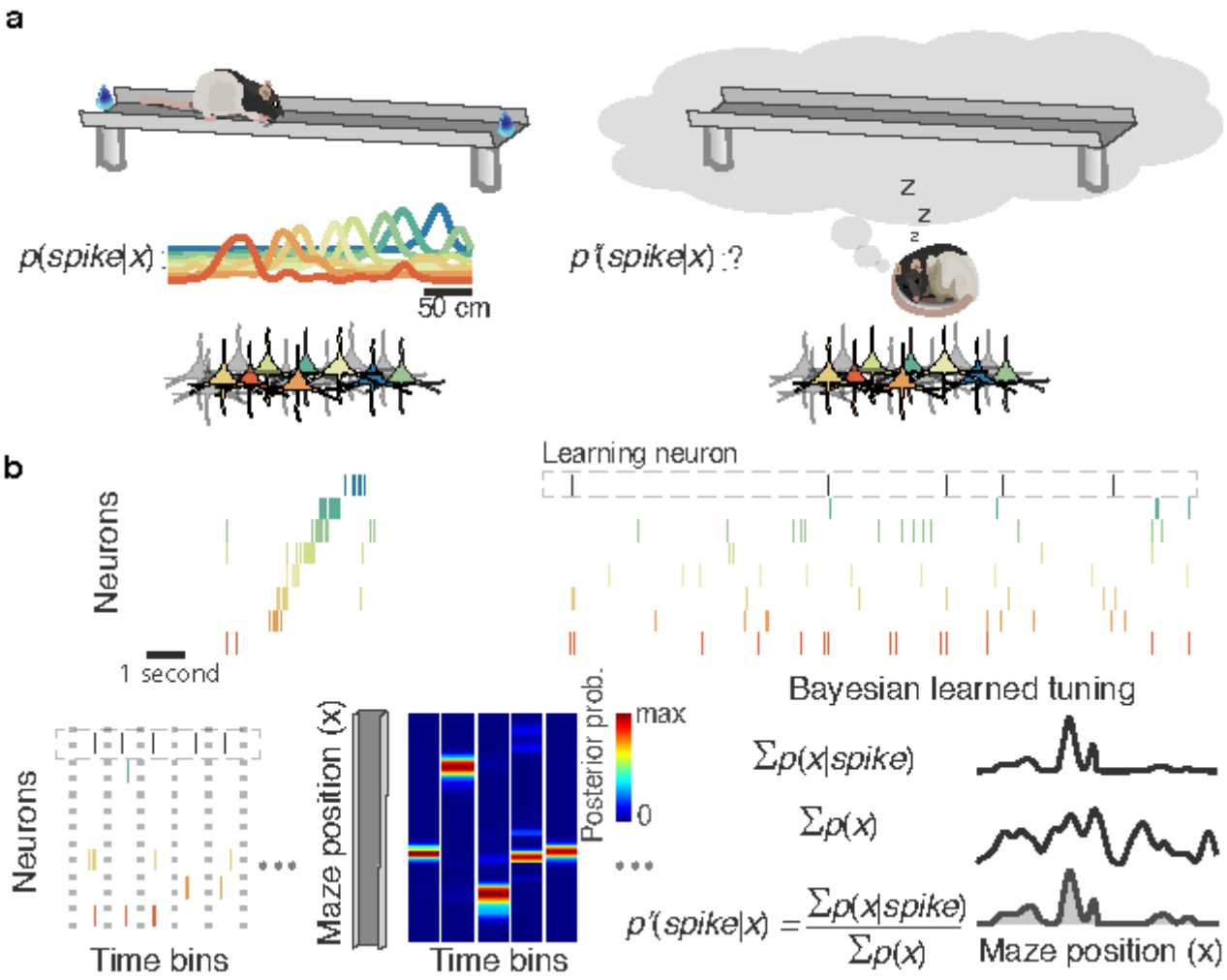

Figure 1

Bayesian learning of hippocampal spatial tunings during offline states.

Figure 2

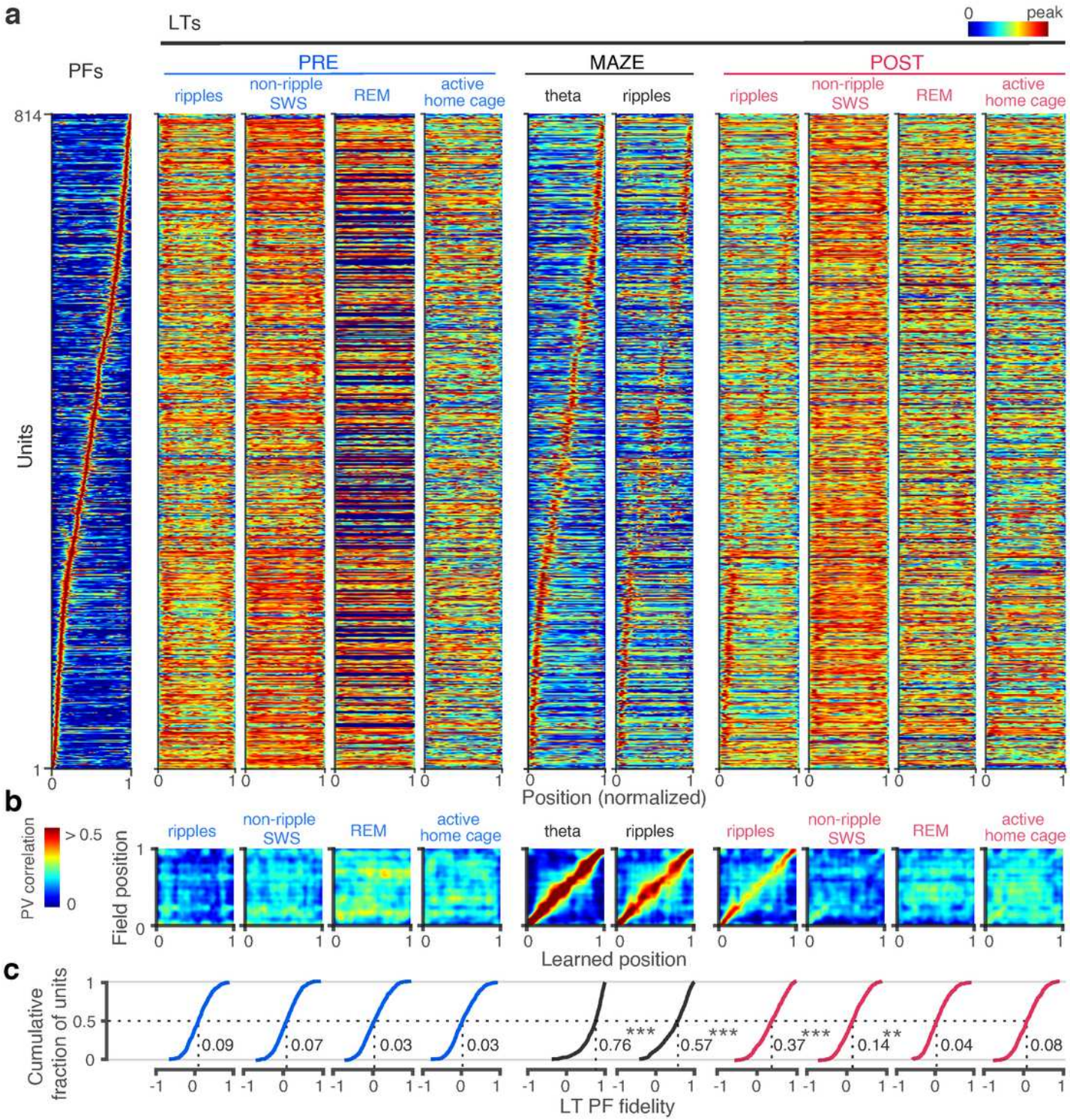

Figure 2

Bayesian learned tunings during MAZE and offline states.

Figure 3

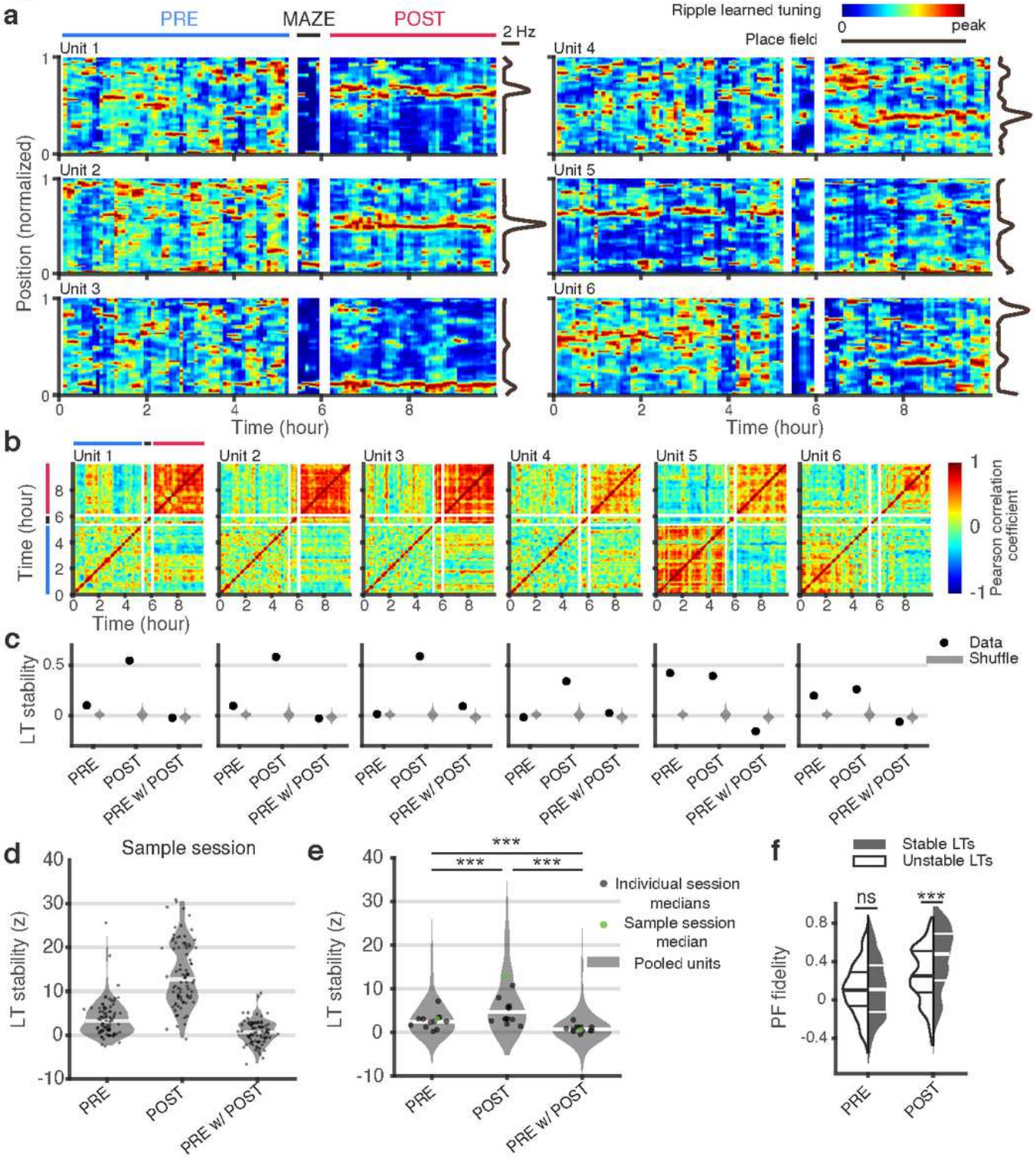

Figure 3

Stability of learned tunings during ripples in PRE and POST.

Figure 4

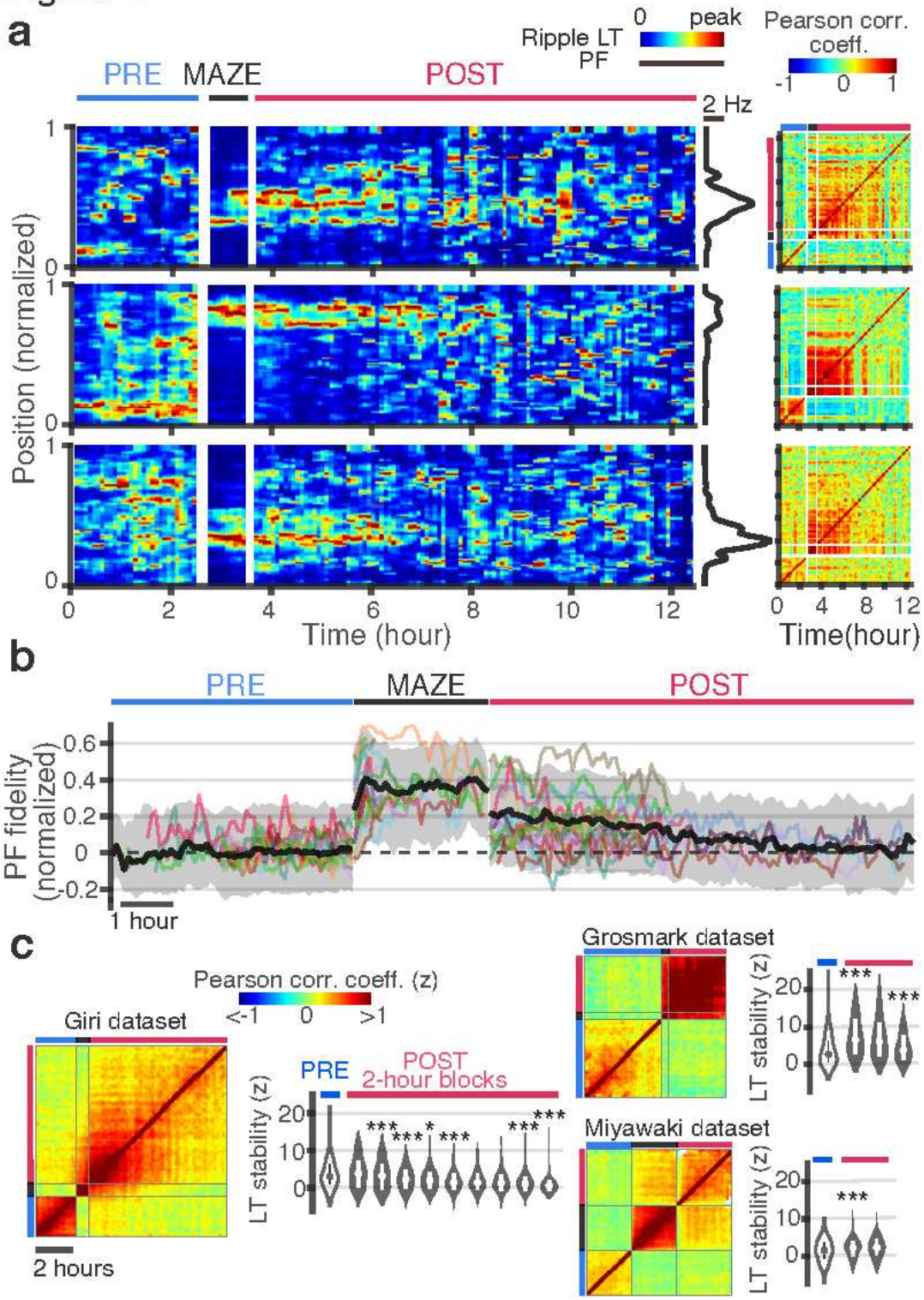

Figure 4

Spatial representations are randomized over the course of sleep.

Figure 5

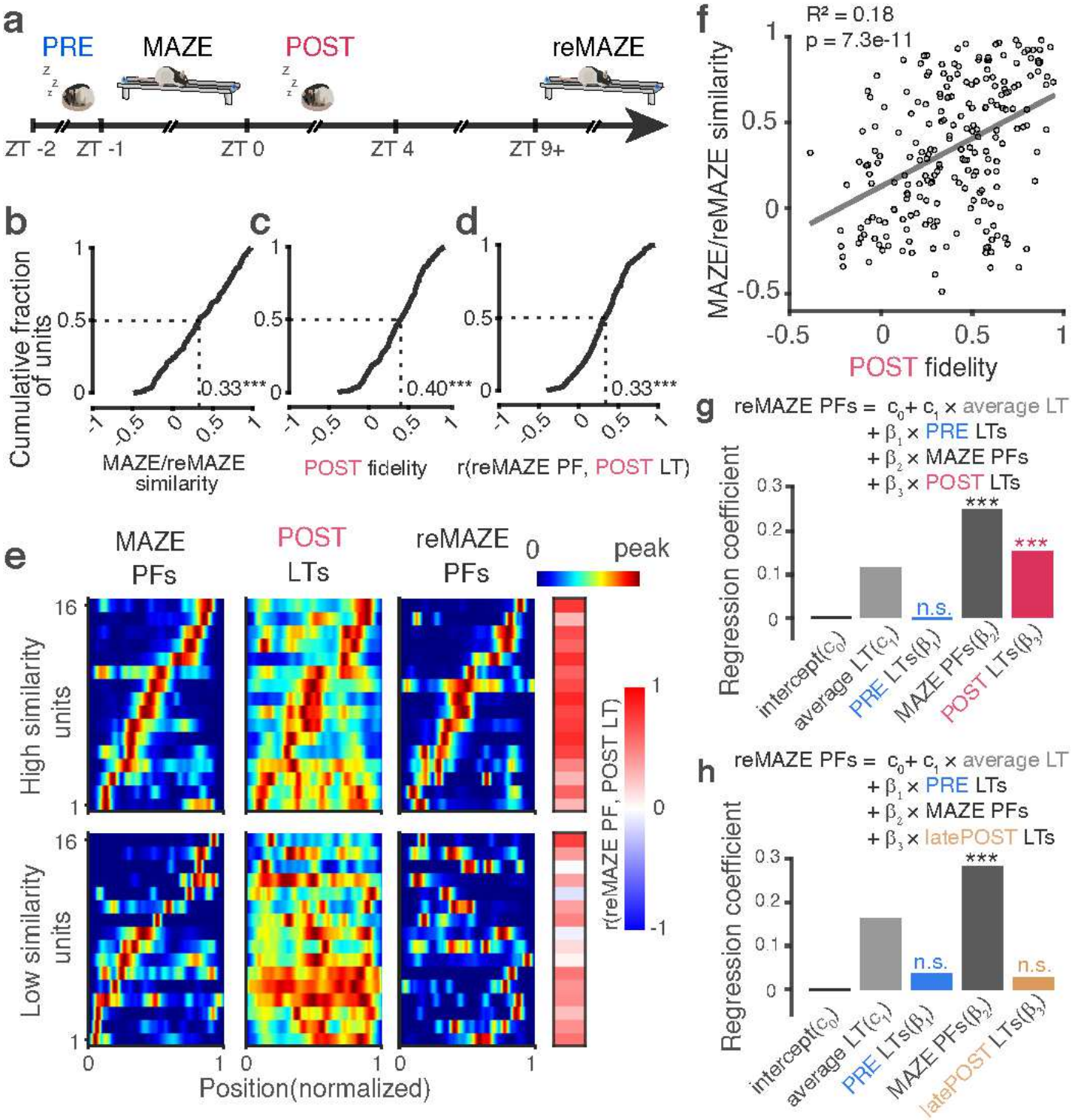

Figure 5

POST ripple tunings predict future place fields on maze re-exposure.

Figure 6

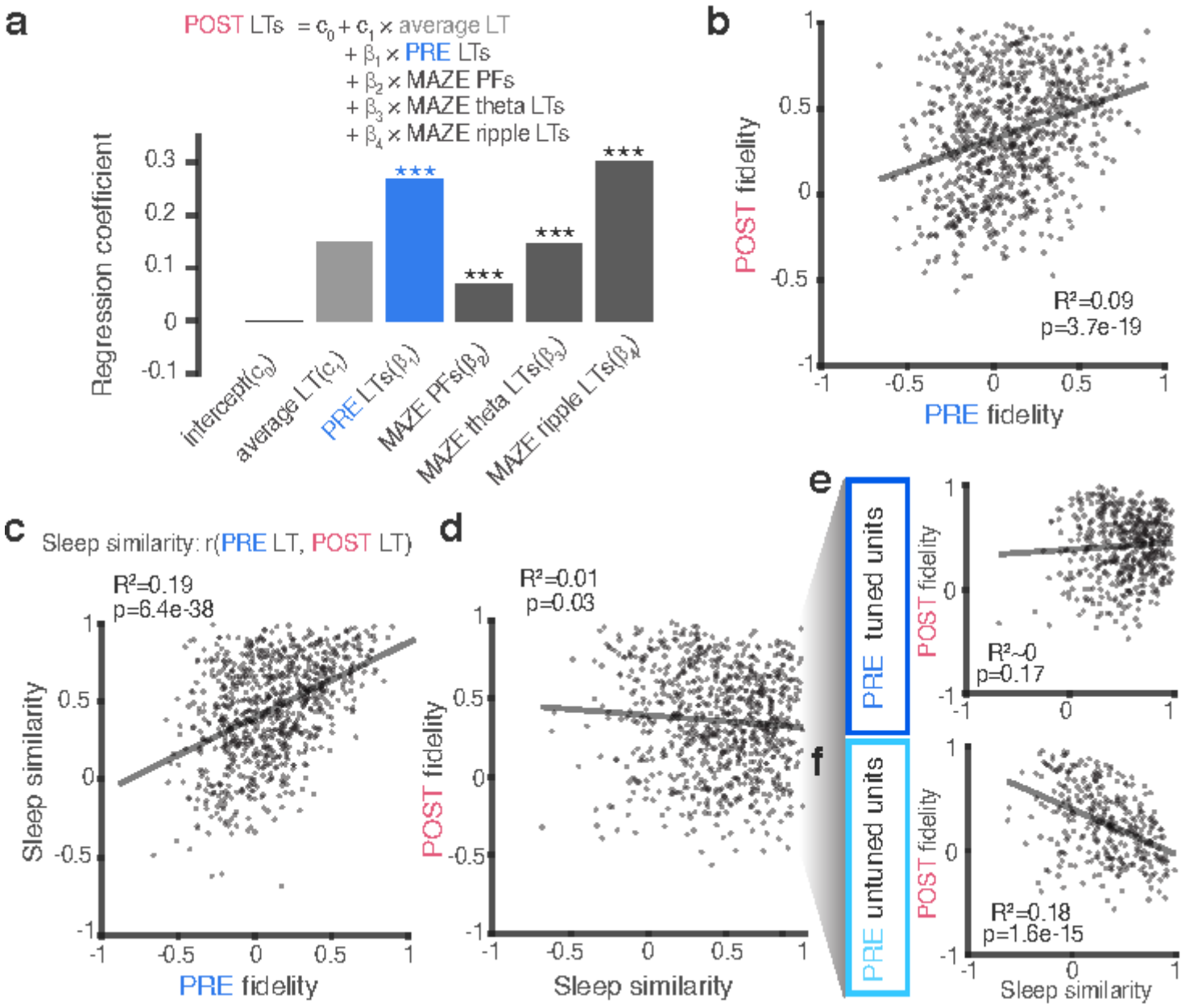

Figure 6

Ensemble patterns during awake theta and ripples and a diversity of pre-existing representations impact the tunings in POST sleep.

Supplementary Files

This is a list of supplementary files associated with this preprint. Click to download.

- ExtendedDataFig1.pdf
- ExtendedDataFig2.pdf
- ExtendedDataFig3.pdf